Spatio-temporal patterns in ultra-slow domain wall creep dynamics

Ezequiel E. Ferrero
Université Grenoble Alpes, LIPHY, F-38000 Grenoble, France and CNRS, LIPHY, F-38000 Grenoble, France

Laura Foini and Thierry Giamarchi
Department of Quantum Matter Physics, University of Geneva, 24 Quai Ernest-Ansermet, CH-1211 Geneva, Switzerland

Alejandro B. Kolton
Instituto Balseiro-UNCu and CONICET, Centro Atómico Bariloche, 8400 Bariloche, Argentina

Alberto Rosso
LPTMS, CNRS, Univ. Paris-Sud, Université Paris-Saclay, 91405 Orsay, France

In presence of impurities, ferromagnetic and ferroelectric domain walls slide only above a finite external field. Close to this depinning threshold, the wall proceeds by large and abrupt jumps, called avalanches, while, at much smaller field, it creeps by thermal activation. In this work we develop a novel numerical technique that captures the ultra-slow creep regime over huge time scales. We point out the existence of activated events that involve collective reorganizations similar to avalanches, but, at variance with them, display correlated spatio-temporal patterns that resemble the complex sequence of aftershocks observed after a large earthquake. Remarkably, we show that events assembly in independent clusters owning the same scale-free statistics as critical depinning avalanches. This correlated dynamics should be experimentally accessible by magneto-optical imaging of ferromagnetic films.

Ferromagnetic [1–4] and ferroelectric [5, 6] domains display a strong non-linear response to the application of an external drive. Any small perturbation can induce a large and random rearrangement, called avalanche. The fate of the perturbation is controlled by the strength of the external field. Above a finite threshold a never-ending avalanche is triggered and the entire system polarizes. Below threshold avalanches remain finite and dynamics is limited to a transient motion. Only at the depinning threshold avalanches become scale free and display universal features [7–9]. A remarkable signature of this critical behavior is provided by the power law noise spectrum measured in Barkhausen experiments [10–12].

Well below threshold the only way to induce macroscopic rearrangements is via thermal activation. In ferromagnetic domains such dynamics is directly imaged thanks to magneto-optic Kerr effect [1, 13]. These experiments show that, when a small drive is applied, the ferromagnetic domain remains pinned in deep metastable configurations, even at room temperature, and displays only incoherent, small-scale, vibrations. However, on very long time scales, a collective creep dynamics associated to a slow domain growth is observed [1, 14–16]. The possibility to control or (at least) envisage the rate of such a growth has deep applications for the design of new devices as, for example, magnetic racetrack memories [17–19]. Unfortunately, though, our understanding of this creep dynamics remains limited to few phenomenological arguments and many relevant questions are still open: At which velocity the domain grows? Which length scales are involved? Shall we expect universality to hold in this regime?

Answering these questions amounts to describe the slow glassy dynamics of a strongly interacting disordered system. A key simplification comes from the experimental observation that nucleation of new domains is negligible and the motion is restricted to the dynamics of the wall separating regions with opposite magnetization. Nonetheless the numerical study of the creep regime of a single interface remains a big challenge, as most of the thermal excitations produce incoherent deformations that are rapidly dissipated. Only very rarely these excitations find a pathway that produce forward motion and domain growth. To overcome these difficulties we decided to focus on the coarse grained dynamics of these rare events where jumps between dynamically stable configurations are performed by thermal activation. This procedure allowed us to explore very small values of the external drive revealing the essential features of the creep regime.

Our results are consistent with the well-known creep formula for the velocity-force characteristics. This formula was first derived with scaling arguments [20–23], then confirmed by a functional renormalization group analysis [24] and even tested experimentally [1]. However, beyond the average velocity, the FRG analysis clearly showed [14, 24] a more complex physics for the creep *motion* than the scaling picture was suggesting. In that picture, some assumptions were made to obtain the creep formula. Here we invalidate one of them, namely the common belief of a dynamics triggered by a sequence of independent events with a *characteristic* force-dependent size. In fact, our analysis demonstrates that the sizes of the events span a broad distribution,

similar to the one displayed by depinning avalanches, but with an anomalous exponent and a force-dependent cut-off.

Looking at the two sequences of events shown in Fig.1 one immediately grasp a fundamental novel feature of creep events (on the left) with respect to depinning avalanches (on the right). Both reorganizations are extended objects involving a large portion of the interface, but their spatio-temporal arrangement is very different: depinning avalanches randomly nucleate all along the interface while creep events cluster around an initial seed. This behavior is similar to what is observed in earthquakes dynamics where, after a main shock, a large sequence of aftershocks is recorded [25]. Interestingly, the analysis of creep patterns shows that the size of these uncorrelated clusters becomes truly scale free and characterized by the same exponents of the depinning transition.

The rest of the paper is organized as follows. We first describe the elastic interface model and provide the scaling arguments characterizing the dynamics in the creep regime and at the depinning transition. Then, we introduce our coarse-grained dynamics and discuss our main findings. We conclude with a discussion and perspectives. Some complementary results and details of our analysis are collected in the Supplementary Information (SI).

I. THE MODEL: ELASTIC INTERFACES IN RANDOM MEDIA

We consider a d-dimensional wall separating two $d+1$-dimensional domains of opposite polarization. For simplicity we model it as an oriented interface displacing only along the perpendicular direction h. Thus, at any time t, the wall is described by a single valued function $h(x,t)$ (the transverse displacement h of the interface at longitudinal position x) and the possibility of overhangs is neglected. In most of the cases, viscosity dominate over inertia and the local velocity of the wall is given by

$$\gamma \partial_t h(x,t) = c\nabla^2 h(x,t) + f + F_{\rm p}(x,h) + \eta(x,t) \qquad (1)$$

where $c\nabla^2 h(x,t)$ describes the elastic force arising from the domain wall surface tension, f is proportional to the external field pulling the wall, and the fluctuations due to randomly distributed impurities and temperature are encoded in the quenched stochastic term $F_{\rm p}(x,h)$ and in the Langevin thermal noise $\eta(x,t)$ respectively. This coarse grained equation, so called quenched Edwards-Wilkinson equation, is a minimal model supposed to govern the universal wall dynamics at large scales [9, 26, 27]. The parameters of Eq.1, describing intrinsic properties of the wall, can be directly related to microscopic properties of the host material. For example, in ferromagnetic thin films c depends on the strength of magnetic exchange interactions, the strength of magnetic anisotropy and sample thickness, while γ can be related to dissipative processes such as the micromagnetic damping [13]. Concerning the quenched term, two classes of disorder are physically relevant: (i) In the Random Force class (RF), induced by random quenched local magnetic fields, the pinning force $F_p = -\partial_h V_d(x,h)$ displays short range correlations while the pinning potential $V_d(x,h)$ displays long-range correlations in the direction of displacements. (ii) In the Random Bond class (RB), induced, for instance, by local spatial fluctuations of the magnetic exchange interactions or by fluctuations of the the magnetic anisotropy, both the pinning potential and the pinning force are short-ranged correlated in the direction of displacements. In both cases we assume the absence of correlations along the x direction.

The response of the interface to an external drive recalls the behavior of a continuous phase transition. It can be explained as follows.

At zero temperature ($T=0$) the threshold f_c separates the regime where the interface is pinned (velocity $V=0$, $f<f_c$) from the regime where a steady motion can be observed ($V>0$, $f>f_c$). At finite temperature the steady state movement is also possible below f_c, through thermally activated events. See Fig.2 for a schematic view of the velocity-force characteristics. At zero temperature there are two critical points where self-affinity and scale-free behavior are expected:

Equilibrium scaling. The first, at $f=0$, corresponds to thermodynamic equilibrium where the extensive ground state energy displays critical sample to sample fluctuations, growing as $L^{\theta_{\rm eq}}$ and the domain wall is rough with a self-affine width growing as $L^{\zeta_{\rm eq}}$ (see Fig.2 at $f=0$). At equilibrium, a slow annealing of a parameter of Eq.1 induces sudden rearrangements of the interface. The comprised area S between two subsequent ground states (a measure of the rearrangement size) is a random variable with power law statistics $P(S) \sim S^{-\tau_{\rm eq}}$ below a cut-off size S_c controlled by the system size as $S_c \sim L^{d+\zeta_{\rm eq}}$. The scale free exponent $\tau_{\rm eq}$ was shown to be related with the equilibrium roughness exponent as [28] $\tau_{\rm eq} = 2 - 2/(d+\zeta_{\rm eq})$. The exponents $\theta_{\rm eq}$ and $\zeta_{\rm eq}$ are universal and depend on dimension, range of elastic interactions and class of the disorder.

Depinning scaling. The second critical point, at $f=f_c$ and zero temperature, corresponds to the depinning transition above which the interface acquires a finite global velocity $V \sim (f-f_c)^{\beta_{\rm dep}}$. This depinning critical point is characterized by a roughness $\zeta_{\rm dep}$ (see Fig.2 at $f=f_c$). At any force close to f_c a small perturbation can induce a large reorganization of the interface, called depinning avalanche. As in equilibrium, the avalanche size S (redefining S), namely the area spanned by the moving interface, has also a power-law statistics, but different exponents:

$$P(S) \sim S^{-\tau} G(S/S_c) \qquad (2)$$

where the cut-off S_c is controlled by the system size $S_c \sim L^{d+\zeta_{\rm dep}}$. Remarkably, as in equilibrium, it is possible again to relate the scale free exponent τ with the cut-off

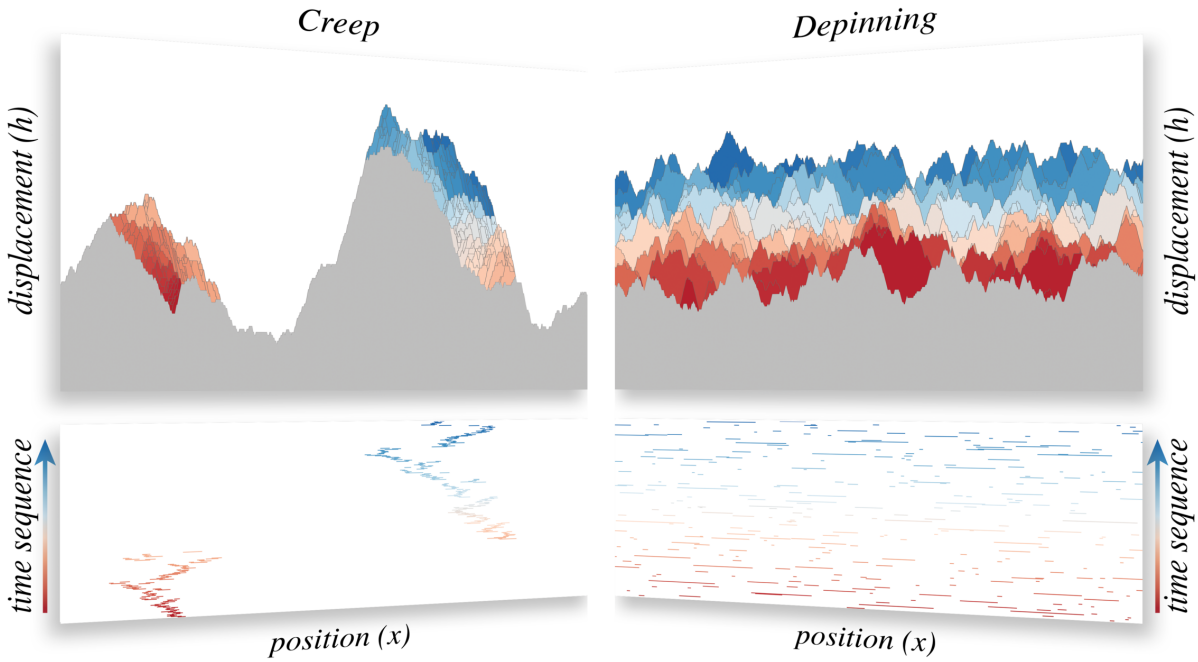

FIG. 1: *Spatio-temporal patterns: Creep (left) versus Depinning (right)*– Top row: Snapshot of 300 consecutive configurations for the moving interface. At a small force ($f = 0.05$), in the creep regime, thermal fluctuations trigger a sequence of events while, at much larger force, ($f \simeq f_c \sim 1$), close to depinning, the interface responds to small perturbations with deterministic avalanches. Bottom row: The activity map is composed by horizontal segments depicting the location of the sites involved in the same event or avalanche. The time sequence illustrates the used color code: dark red correspond to old creep events (respectively depinning avalanches) and dark blue correspond to the more recent ones. The two dynamical regimes appear qualitatively very different: depinning avalanches are uncorrelated, while the activated events clearly assemble in two independent clusters.

exponent $d + \zeta_{\rm dep}$ [29, 30]:

$$\tau = \tau_{\rm dep} = 2 - \frac{2}{d + \zeta_{\rm dep}} \tag{3}$$

Away from criticality, a finite correlation length $\ell(f) \sim |f - f_c|^{-\nu_{\rm dep}}$ is measured with $\nu_{\rm dep} = 1/(2 - \zeta_{\rm dep})$. Below threshold, the presence of the scale $\ell(f)$ modifies the avalanche cut-off $S_c(f) \sim f^{-\alpha} \sim \ell(f)^{d+\zeta_{\rm dep}}$, but leaves the critical exponents in Eq.2 unchanged.

At small but *finite* temperature ($T > 0$) and below f_c the dynamics appears as a collection of incoherent vibrations localized around deep metastable configurations. However, the presence of a small positive drive makes a global forward motion energetically favorable and the dynamics is well described by the creep scaling: In order to move a portion ℓ^d of the interface across disorder it is necessary to improve a configurational energy that scales as $\ell^{\theta_{\rm eq}}$, with $\theta_{\rm eq}$ a characteristic exponent of equilibrium. On the other hand, the energetic gain due to the applied force scales as $f\,\ell^{d+\zeta_{\rm eq}}$. The balance between these two contributions indicates that the minimal length scale above which the total energy would be irreversibly lowered diverges when $f \to 0$ as

$$L_{\rm opt}(f) \sim 1/f^{\nu_{\rm eq}} \quad \text{with} \quad \nu_{\rm eq} = \frac{1}{d + \zeta_{\rm eq} - \theta_{\rm eq}} \tag{4}$$

From this scaling argument, and the additional idea that the deterministic flow of the interface is made of a sequence of activated events of typical size $L_{\rm opt}$, its velocity can be determined using the Arrhenius formula for the activation time Δt [20, 21]:

$$V = \frac{\Delta h}{\Delta t} \sim L_{\rm opt}^{\zeta}\, e^{-\frac{L_{\rm opt}^{\theta}}{k_B T}} \sim \exp\left(-\frac{U_c}{k_B T}\left(\frac{\tilde{f}_c}{f}\right)^{\mu}\right). \tag{5}$$

Here, $\tilde{f}_c$ and U_c are two microscopic parameters, and $\mu = \nu_{\rm eq}\theta = \theta/(d + \zeta_{\rm eq} - \theta_{\rm eq})$ (see Fig. 2 at $f \ll f_c$). This result for the velocity is supported by the FRG analysis [24]. The general assumption is that all the exponents entering in the above creep formula are the ones of equilibrium, but its validity is not obvious for two reasons: (i) the interface is in a steady state far from equilibrium, and (ii) the exponent $\theta_{\rm eq}$ characterizes the fluctuations of ground state energies, while θ in Eq.5 is associated to the energetic barriers to overcome. The hypothesis that $\theta = \theta_{\rm eq}$ was tested time ago by Drossel *et al* [31] despite criticism [32]. Moreover, experiments on magnetic

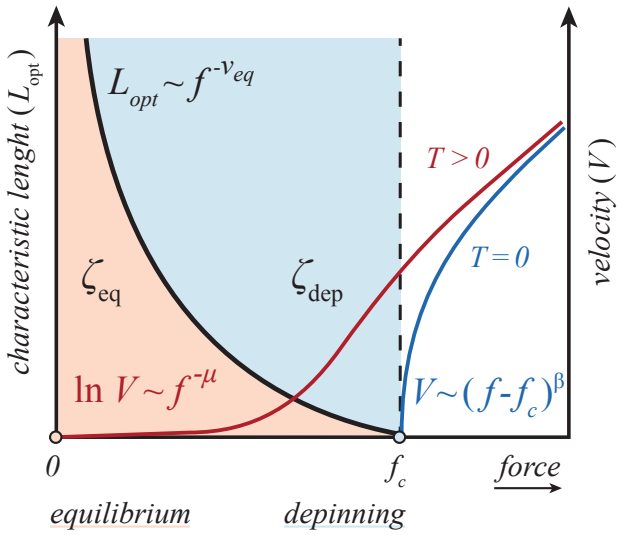

FIG. 2: *Velocity-force characteristics, dynamical regimes and fixed points* – The figure shows schematically two aspects of the $T > 0$ steady state dynamics of the elastic interface below f_c: (i) The velocity V, strictly equal to zero in the $T = 0$ case, has a finite value that at low forces is well approximated by the creep law $V \sim \exp(f^{-\mu})$, with $\mu > 0$ the creep exponent. (ii) A characteristic length scale $L_{\rm opt}$, that diverges as f goes to zero, separates two dynamical regimes identified by different roughness exponents. Below $L_{\rm opt}$ the interface, with roughness $\zeta_{\rm eq}$, appears to be at the equilibrium fixed point, while above $L_{\rm opt}$ the interface, with roughness $\zeta_{\rm dep}$, appears to be at the critical depinning point.

domain wall motion [1, 13, 33, 34] show a stretched exponential behavior of the velocity as a function of the force with shape exponent $\mu = 1/4$, in agreement with the equilibrium exponents [35] for $d = 1$ ($\theta_{\rm eq} = 1/3$, $\zeta_{\rm eq} = 2/3$). Further analysis of the FRG equations [36] suggests that a second lengthscale appears in the creep motion. In the following we will show that our steady state simulations support the hypothesis that creep is made of a sequence of activated events well described by equilibrium exponents, but that such a sequence is statistically very different from the one assumed by the above scaling arguments (uncorrelated events of a well defined typical size).

II. MODEL FOR T=0+ DYNAMICS

The numerical study of Eq.1 in the creep regime is particularly challenging [27]. Traditional integration schemes, like molecular dynamics, fail to capture the long time scales associated to the activated events. We focus here, instead, on a coarse-grained dynamical approach that targets the rare events that move the interface forward irreversibly (i.e., we replace the infinite time sampling of new possible configurations by choosing explicitly the most probable one). The motion corresponds therefore to a sequence of metastable states of decreasing energy separated by energy barriers that eventually account for the real time delay of the transitions.

At vanishing temperature it was shown [16] that the choice of the next metastable state amounts to find the minimal energy barrier to be overcome to allow forward motion. This corresponds to enumerate all pathways that end in a state with lower energy and select the one that overcome the smallest barrier. Unfortunately this protocol is very expensive, its computing time grows exponentially with $L_{\rm opt}$. In order to explore the low force regime, where creep scaling laws should apply and $L_{\rm opt}$ is very large, we adopted a different strategy. Our approach consists in asking, given a metastable configuration, for the minimum rearrangement (in size) that takes the interface to a lower energy state. At small forces this is equivalent to search for a minimal barrier since they grow extensively with the size of the rearrangement $\sim \ell^{\theta}$. With this prescription we can compute the sequence of metastable states using an efficient algorithm developed for the directed polymer on a lattice.

The dynamics that evolves the polymer from one metastable state to the next one is composed by two steps: an *activated move* to jump the barrier, using the above described approximation, followed by a *deterministic relaxation*, that drives the polymer through the energy lowering gradient till the next minimum is reached. The details of our dynamics and parallel implementation are given in the SI. This strategy allows us to decrease the force a factor 100 compared to previous works [15, 16], unveiling a novel dynamical regime.

III. NUMERICAL RESULTS

The output of the coarse grained dynamics, as shown in Fig.1, is a sequence of metastable states separated by a compact region that we call event. The size, S, of each event corresponds to the area of such a region. From the traditional picture of creep dynamics, one would expect that for small driving forces the event size fluctuates around a typical value $L_{\rm opt}^{d+\zeta_{\rm eq}}$. However, in Fig.3-left, we show that the event size distribution displays an unexpected power law scaling similar to the depinning one of Eq.2, with a force dependent cut off. A good collapse is found for $S_c(f) \sim f^{-\alpha}$ with $\alpha = 1.25$, a value perfectly consistent with the behavior of $S_{\rm opt} \sim L_{\rm opt}^{d+\zeta_{\rm eq}}$, implying for d=1 $\alpha = (d + \zeta_{\rm eq})\nu_{\rm eq} = 5/4$ and therefore, $S_c \sim S_{\rm opt}$. We conclude that at variance with standard scaling, the characteristic lenght $L_{\rm opt}$ (shown in Fig.2) corresponds to the "largest", rather than the "typical" size of the irreversible events. However the creep law (5) is not affected as, for activated dynamics, the velocity is controlled by the largest barriers and then by $L_{\rm opt}$.

A second important feature of $P(S)$ is the power law decay. A scaling argument, valid for elastic systems [28],

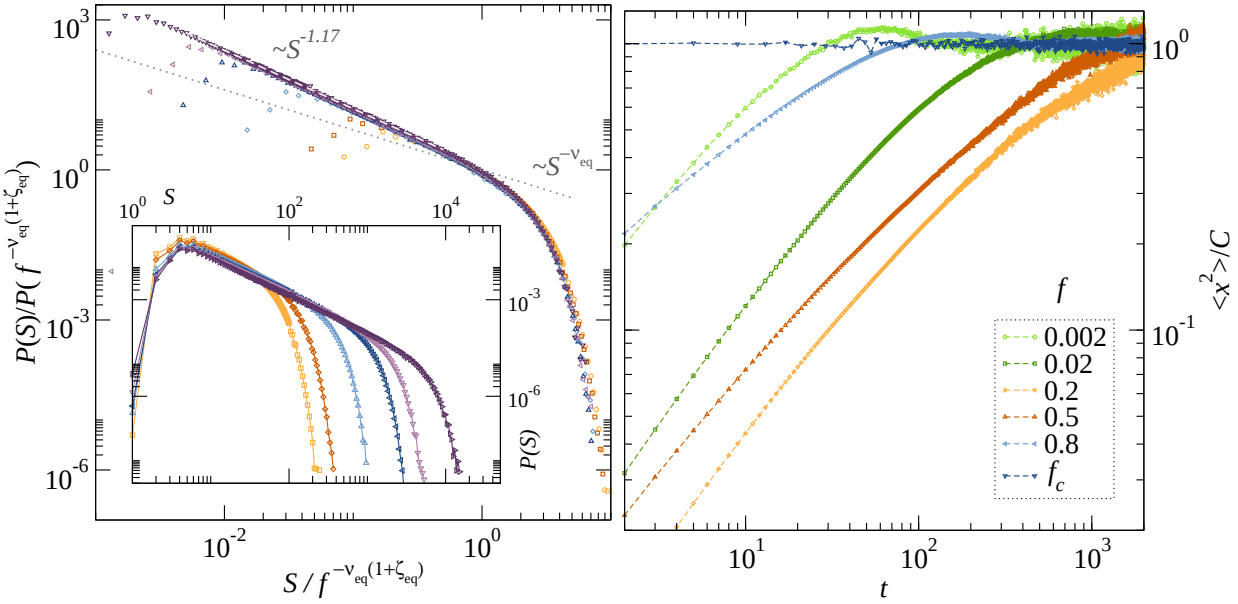

FIG. 3: *Creep dynamics analysis: events size distributions (left) and events location mean-square displacement (right)* – On the left: Events size distributions $P(S)$ *vs.* S at different forces $f = \{0.08, 0.05, 0.02, 0.008, 0.005, 0.002\}$, ranged respectively from left to right in the inset. The main panel show a good collapse of the same curves when plotting $P(S)/P(S_c)$ vs S/S_c with $S_c(f) = f^{-\nu_{\rm eq}(1+\zeta_{\rm eq})}$, therefore validating the expected creep scaling $L_{\rm opt} \sim f^{-\nu_{\rm eq}}$, given $S_c \sim L_{\rm opt}^{(1+\zeta_{\rm eq})}$. Data correspond to a system size $L = 3360$. On the right: Mean square displacement (MSD) $\langle x^2 \rangle$ of the events epicenter as a function of the observed window t (a discrete time distance in the ordered events sequence) for different forces. Correlations among consecutive events render the MSD non trivial in a force dependent time window. Fully uncorrelated events (as the ones for $f = f_c$) can only build a flat MSD, at the system size-dependent asymptotic value $C = (L+1)(L+2)/12$. Data correspond to a system size $L = 960$.

suggests that the cut-off exponent α and the power law exponent τ should satisfy the relation $\tau = 2 - \frac{2\nu_{\rm eq}}{\alpha} = 2 - 2/(d + \zeta_{\rm eq})$. Here the cut-off $\sim f^{-\alpha}$ is controlled by the distance to equilibrium $f = 0$ and we would expect the value $\tau = \tau_{\rm eq} = 4/5$. However this is not the case and we find a larger exponent $\tau = 1.17 \pm 0.01$. Such a distribution with $\tau > \tau_{\rm eq}$, violating the scaling relation, expresses an excess of small events compared to what is expected *a priori* for a distribution of fully independent avalanches.

To shed light on this issue, we further inspect Fig. 1. We observe that creep events are organized in compact spatio-temporal patterns while depinning avalanches appear randomly distributed along the interface, as is well illustrated by the activity maps that supplement the sequence of metastable configurations. In order to make this comparison more quantitative we analyze the degree of correlation among creep events by computing the mean squared displacement (MSD), $\langle \Delta X^2(t) \rangle$, of the (epicenter) location of events separated by t metastable states. In absence of correlations we expect $\langle \Delta X^2(t) \rangle = C$ with $C = (1/L) \sum_{i=1}^{L/2} 2i^2 = (L+1)(L+2)/12$, for a line of size L. As we show in Fig. 3-right this is well verified by depinning avalanches at all times, while creep events show this behavior only asymptotically for large t. In fact, at short times, the distance among epicenters tends to be small as the events overlap in space, reducing in this way the MSD compared to the uncorrelated case. Furthermore, one sees that for a fixed short time, the MSD displays a non-monotonic behavior as a function of f. This can be understood by considering that for consecutive events overlapping in space the mean distance among their epicenters is controlled by their typical size $L_{\rm eve}(f)$, which has also a non-monotonic behavior with f. In fact, $L_{\rm eve}$ is defined as a combination of an activated move of size $L_{\rm opt}$, which diverges for $f \to 0$, plus a deterministic relaxation diverging at $f \to f_c$. Therefore, $L_{\rm eve}$ diverges at both critical points while taking a minimal value at intermediate forces.

Such short-time correlations between events are similar to the one observed in real earthquakes where a large main shock is followed by a cascade of aftershocks [25, 37]. Due to the presence of these correlations the sequence of events is not homogeneous and the scaling relation between τ and α is not supposed to hold. We find that the effective creep exponent τ is bigger than the value predicted for avalanches at equilibrium and, indeed, this observation holds also for the Gutenberg-Richter exponent, $b = \frac{3}{2}(\tau - 1)$ of real earthquakes. In fact, in absence of correlations the value of b should be smaller

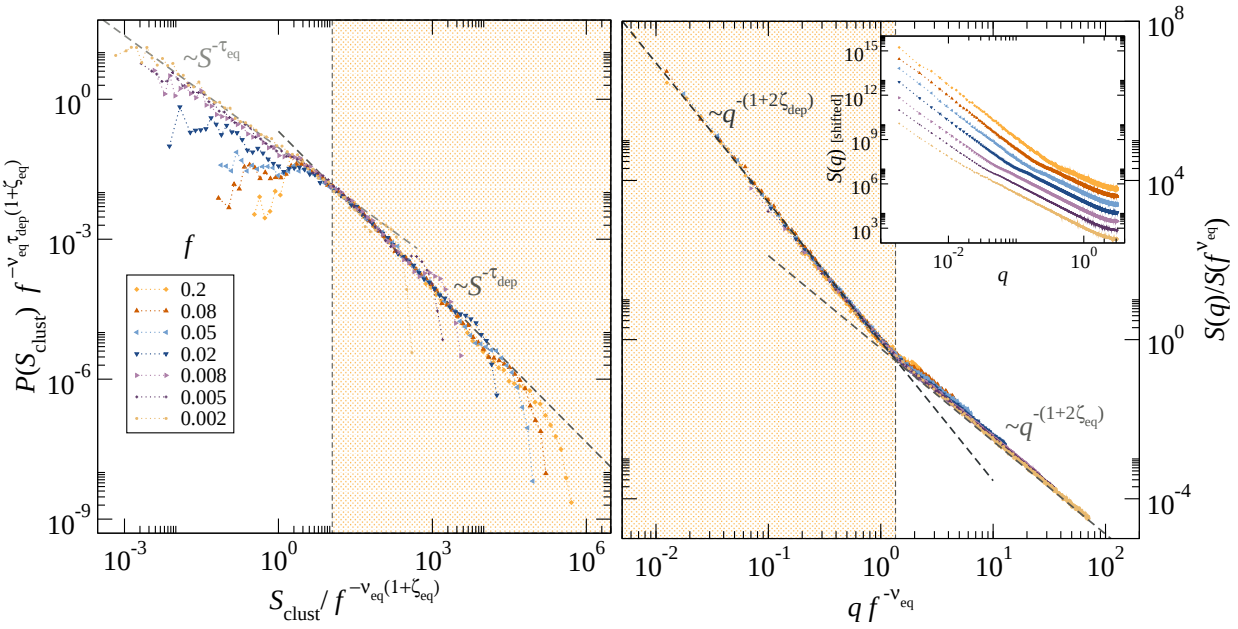

FIG. 4: *Relation between transport and geometry: clusters distributions (left) and interface structure factor (right)* – On the left: Size distribution $P(S_{\rm clust})$ of clusters formed by correlated events, as a function of their size $S_{\rm clust}$ at different forces presented on the labels. A characteristic size $S_c \sim L_{\rm opt}^{(1+\zeta_{\rm eq})}$, with the force-controlled length scale being $L_{\rm opt} \sim f^{-\nu_{\rm eq}}$, separates small clusters that follow an "equilibrium"-like statistics from big clusters that follow a "depinning"-like one. data correspond to a system size $L = 3360$. On the right: Structure factor $S(q)$ of the elastic line, averaged over metastable configurations. The inset shows $S(q)$ as a function of the Fourier mode q for the same forces and labels as in the left panel. The main plot shows the same data rescaled as $S(q)/S(l^{-1})$ *vs.* ql with $l = f^{-\nu_{\rm eq}} \sim L_{\rm opt}$ denoting a geometrical crossover from "equilibrium"-like roughness at small scales to a "depinning"-like roughness at large scales. A secondary geometric crossover at very large (force-dependent) scales, the "anharmonic" crossover, is discussed on the SI. Data correspond to a system size $L = 3360$.

than the mean field prediction 3/4, while from the seismic records one gets $b \simeq 1$ [25, 38].

In order to analyze this spatio-temporal patterns we collect correlated events in *clusters*. In presence of short range elasticity a simple criterion for the cluster formation is to include a new event in the growing cluster if it has a spatial overlap with the cluster. The growth of a cluster stops whenever a new event has no overlap with it. This event, in turn, represents the seed for the creation of a new cluster. In finite systems this procedure can generate system sized clusters, and in this case we decide to break artificially the cluster construction, and start with a new cluster. This occurrence introduces a finite-size effect in the analysis, whose consequences, however, can be kept under control considering bigger systems. The observation of such percolating clusters, in fact, becomes more and more rare for large system sizes.

Upon identifying the sequence of clusters, one has straightforwardly access to their size, i.e. the total area spanned by the interface which is simply the sum of the areas of all the events that compose the cluster. In Fig. 4 we present the cluster size distribution $P(S_{\rm clust})$ which displays a crossover between two power-law decays. The crossover occurs at a scale proportional to $S_{\rm opt}$ as can be seen from the collapse. Below this scale, the power-law in the cluster size distribution shows an exponent 0.80 ± 0.06 corresponding to the equilibrium regime ($\tau_{\rm eq} = \frac{4}{5}$). Clusters of sizes bigger than this scale, instead, are distributed in a power-law fashion with an exponent 1.11 ± 0.04, in good agreement with the depinning criticality [30] $\tau_{\rm dep} \sim 1.11$. In order to span more than eight decades in $S/S_{\rm opt}$, we have simulated a broad range of forces. The equilibrium exponent appears in the limit of small forces, while forces larger than $f \simeq 0.05$ only display the depinning τ with a lower cutoff around $S = S_{\rm opt}$. The upper cut-off of the distribution is controlled by the system size and is expected to disappear in the thermodynamic limit, as can be seen from a finite-size analysis.

In the right panel of Fig. 4 we show the structure factor characterizing the interface. The figure clearly shows a crossover length scale $1/q_c \sim L_{\rm opt}$ that separates short distances (large q) where the structure factor is compatible with the equilibrium roughness and large scales (small q) where the exponents are those of the depinning, as represented schematically in Fig.2. In particular we find $S(q) \propto q^{-\sigma}$ with $\sigma = d{+}2\zeta$ and $\zeta_{\rm eq} = 2/3$ and $\zeta_{\rm dep} = 1.25$ respectively in the two regimes, in agreement with the

values obtained previously at equilibrium [35] and out of equilibrium [16, 39]. The fact that at large distances one recovers the roughness of the depinning is compatible with the observation of the depinning exponent in the clusters size distribution and supports the claim that these objects behave as avalanches at the depinnining critical point. The same $S(q)$ plot had been shown down to forces $f \simeq 0.2$ in a previous work [16]; here it is shown down to $f = 0.002$, which allows to observe a crossover length scale which was barely visible before.

The robustness of all these observations is confirmed by the study of the Random Field disorder case. RF and RB disorder belong to different universality classes at equilibrium, but share the same exponents at the depinning transition [14, 29]. Our results for the creep regime show that the cluster size distribution respects this property, displaying disorder-type dependent equilibrium exponents at scales smaller than $S_{\rm opt}$ and disorder-type independent depinning exponents at scales bigger than $S_{\rm opt}$. In both cases the scaling of $S_{\rm opt}$ with the force is controlled by the corresponding equilibrium exponents (see SI). Altogether, the analysis of the RF disorder corroborates our conclusion that large clusters appear in the thermodynamic limit as avalanches sitting exactly at the critical depinning point with scale free statistics and no cut-off.

Notice that the above picture is complete for an elastic line with unbounded displacement. In our case we have simulated the interface under the hard constraint $|h(x) - h(x+1)| \leq 1$. This constraint introduces an additional length scale $L_{\rm anh}$ beyond which the line enters in the depinning anharmonic regime, characterized by a different roughness exponent [39] $\zeta_{\rm dep}^{\rm anh} = 0.635 \pm 0.005$. For the forces shown in Fig. 4 this crossover occurs at scales comparable to the system size and therefore only the harmonic exponents are visible. However, as can be seen in the SI, we observe that for large enough forces the crossover controlled by $L_{\rm anh}$ is visible, both in the structure factor and in the cluster distribution, and the anharmonic exponents predicted theoretically for this regime are recovered. Moreover, at arbitrarily small force, such a crossover will actually appear in any finite-size analysis for large enough system sizes.

IV. CONCLUSIONS

We have investigated the ultra-slow creep dynamics of an elastic interface moving in a disordered environment subject to small drives and at vanishingly small temperature.

Our results show that at length scales smaller than $L_{\rm opt}$ the system behaves as at equilibrium, while at larger scales, even in presence of a very small force, the emergent properties are those of the depinning universality class. These results are in agreement with a Functional Renormalization Group (FRG) analysis of the problem, that depicts the equilibrium as an unstable fixed point. Indeed, by FRG it was found [14] that the occurrence of an activated event, which is possible thanks to thermal fluctuations, triggers a subsequent depinning-like motion involving a much larger portion of the interface, suggesting the emergence of the two distinct regimes.

Our newly developed algorithm allows us to have an accurate description of the forward irreversible motion of the interface, which advances by activation of large segments overcoming high energy barriers. In particular the algorithm proceeds from one metastable state to the next one, defining in this way the creep "events". Thanks to a well controlled approximation we were able to explore small enough forces and reveal the creep dynamics. In particular we observe that, contrary to the common belief, the sizes of the creep events do not fluctuate around a typical value but instead they are distributed in a power-law fashion, with an anomalous exponent.

The most striking property that emerges from the analysis of these events is, though, their occurrence in correlated spatio-temporal patterns, in sharp contrast with depinning and static avalanches which, instead, nucleate randomly along the line. Noteworthy, even if these results invalidate one of the original assumptions [20, 22, 23, 40] behind the phenomenological derivation of the creep velocity, the observation of a cutoff length scale for the event size distribution precisely scaling as $L_{\rm opt} \sim f^{-\nu_{\rm eq}}$ leads to the same scaling arguments that yields the creep law.

In order to deepen our understanding of such a correlated dynamics we have constructed collective objects that we call "clusters" (the union of subsequent events that overlap in space). Quite remarkably, the statistical properties of these extended objects beyond a crossover length governed by $L_{\rm opt}$ closely resemble those of independent depinning avalanches, confirming that the physics at large scales is dominated by the depinning critical point.

We are confident that this clustering behavior of creep events can be observed in experiments with the current apparatus and techniques if properly sought, and our predictions can be tested. In particular, in line with [41], we are able to predict quantitative values for the length scales that should be considered in Co/Pt/Co ferromagnetic domain wall experiments (we invite the reader to see the Supplementary Information).

ACKNOWLEDGMENTS

E.E.F acknowledge financial support from ERC Grant No. ADG20110209 (GLASSDEF, J.-L. Barrat). A.B.K. acknowledges partial support from Projects CONICET-PIP11220120100250CO and ANPCyT-PICT-2011-1537 (Argentina). This work was supported in part by the Swiss SNF under Division II. Most of the computations were performed using the Froggy platform of the CIMENT infrastructure supported by the Rhône-Alpes region (Grant No. CPER07-13 CIRA) and the

Equip@Meso project (Reference No. ANR-10- EQPX-29-01). Further, we would like to warmly thank S. Bustingorry, J. Curiale, E. A. Jagla, V. Jeudy, V. Lecomte, and A. Mougin for fruitful discussions.

[1] S. Lemerle, J. Ferré, C. Chappert, V. Mathet, T. Giamarchi, and P. Le Doussal, Phys. Rev. Lett. **80**, 849 (1998).
[2] M. Yamanouchi, D. Chiba, F. Matsukura, T. Dietl, and H. Ohno, Physical review letters **96**, 096601 (2006).
[3] P. Metaxas, J. Jamet, A. Mougin, M. Cormier, J. Ferré, V. Baltz, B. Rodmacq, B. Dieny, and R. Stamps, Physical Review Letters **99**, 217208 (2007).
[4] V. Repain, M. Bauer, J.-P. Jamet, J. Ferré, A. Mougin, C. Chappert, and H. Bernas, EPL (Europhysics Letters) **68**, 460 (2004).
[5] T. Tybell, P. Paruch, T. Giamarchi, and J.-M. Triscone, Phys. Rev. Lett. **89**, 097601 (2002).
[6] P. Paruch and J.-M. Triscone, Applied physics letters **88**, 162907 (2006).
[7] L.-H. Tang and H. Leschhorn, Phys. Rev. A **45**, R8309 (1992).
[8] M. Paczuski, S. Maslov, and P. Bak, Phys. Rev. E **53**, 414 (1996).
[9] D. S. Fisher, Physics reports **301**, 113 (1998).
[10] H. Barkhausen, Phys. Z **20**, 401 (1919).
[11] S. Zapperi, P. Cizeau, G. Durin, and H. E. Stanley, Physical Review B **58**, 6353 (1998).
[12] G. Durin and S. Zapperi, Physical Review Letters **84**, 4705 (2000).
[13] J. Ferré, P. J. Metaxas, A. Mougin, J.-P. Jamet, J. Gorchon, and V. Jeudy, Comptes Rendus Physique **14**, 651 (2013), disordered systems / Systèmes désordonnés.
[14] P. Chauve, T. Giamarchi, and P. Le Doussal, Phys. Rev. B **62**, 6241 (2000).
[15] A. B. Kolton, A. Rosso, and T. Giamarchi, Phys. Rev. Lett. **94**, 047002 (2005).
[16] A. B. Kolton, A. Rosso, T. Giamarchi, and W. Krauth, Phys. Rev. B **79**, 184207 (2009).
[17] S. S. Parkin, M. Hayashi, and L. Thomas, Science **320**, 190 (2008).
[18] T. Hayward, Scientific reports **5**, 13279 (2015).
[19] S. DuttaGupta, S. Fukami, C. Zhang, H. Sato, M. Yamanouchi, F. Matsukura, and H. Ohno, Nature Physics (2015), 10.1038/nphys3593.
[20] L. Ioffe and V. Vinokur, Journal of Physics C: Solid State Physics **20**, 6149 (1987).
[21] T. Nattermann, EPL (Europhysics Letters) **4**, 1241 (1987).
[22] M. V. Feigel'man, V. B. Geshkenbein, A. I. Larkin, and V. M. Vinokur, Phys. Rev. Lett. **63**, 2303 (1989).
[23] T. Nattermann, Y. Shapir, and I. Vilfan, Phys. Rev. B **42**, 8577 (1990).
[24] P. Chauve, T. Giamarchi, and P. Le Doussal, EPL (Europhysics Letters) **44**, 110 (1998).
[25] C. H. Scholz, The mechanics of earthquakes and faulting (Cambridge university press, 2002).
[26] M. Kardar, Physics Reports **301**, 85– (1999).
[27] E. E. Ferrero, S. Bustingorry, A. B. Kolton, and A. Rosso, Comptes Rendus Physique **14**, 641 (2013).
[28] P. Le Doussal, A. A. Middleton, and K. J. Wiese, Physical Review E **79**, 050101 (2009).
[29] O. Narayan and D. S. Fisher, Physical Review B **48**, 7030 (1993).
[30] A. Rosso, P. Le Doussal, and K. J. Wiese, Physical Review B **80**, 144204 (2009).
[31] B. Drossel and M. Kardar, Phys. Rev. E **52**, 4841 (1995).
[32] C. Monthus and T. Garel, Journal of Physics A: Mathematical and Theoretical **41**, 115002 (2008).
[33] K.-J. Kim, J.-C. Lee, S.-M. Ahn, K.-S. Lee, C.-W. Lee, Y. J. Cho, S. Seo, K.-H. Shin, S.-B. Choe, and H.-W. Lee, Nature **458**, 740 (2009).
[34] J. Gorchon, S. Bustingorry, J. Ferré, V. Jeudy, A. Kolton, and T. Giamarchi, Phys. Rev. Lett. **113**, 027205 (2014).
[35] M. Kardar, Phys. Rev. Lett. **55**, 2923 (1985).
[36] P. Chauve, T. Giamarchi, and P. Le Doussal, Phys. Rev. B **62**, 6241 (2000).
[37] L. Arcangelis, C. Godano, J. R. Grasso, and E. Lippiello, to be published in Physics Report (2016).
[38] E. Jagla, F. P. Landes, and A. Rosso, Physical review letters **112**, 174301 (2014).
[39] A. Rosso, A. K. Hartmann, and W. Krauth, Phys. Rev. E **67**, 021602 (2003).
[40] T. Nattermann, Phys. Rev. Lett. **64**, 2454 (1990).
[41] V. Jeudy, A. Mougin, S. Bustingorry, W. S. Torres, J. Gorchon, A. Kolton, A. Lemaître, and J.-P. Jamet, arXiv preprint arXiv:1603.01674 (2016).
[42] A. B. Kolton, A. Rosso, T. Giamarchi, and W. Krauth, Phys. Rev. Lett. **97**, 057001 (2006).
[43] A. Rosso and W. Krauth, Computer Physics Communications **169**, 188 (2005), proceedings of the Europhysics Conference on Computational Physics 2004.
[44] D. S. Fisher, Phys. Rev. Lett. **56**, 1964 (1986).
[45] P. Chauve, P. Le Doussal, and K. Jörg Wiese, Phys. Rev. Lett. **86**, 1785 (2001).
[46] E. E. Ferrero, S. Bustingorry, and A. B. Kolton, Phys. Rev. E **87**, 032122 (2013).
[47] A. Rosso and W. Krauth, Phys. Rev. Lett. **87**, 187002 (2001).
[48] J. Lin, E. Lerner, A. Rosso, and M. Wyart, **111**, 14382 (2014).
[49] G. Blatter, M. Feigel'Man, V. Geshkenbein, A. Larkin, and V. M. Vinokur, Rev. Mod. Phys. **66**, 1125 (1994).
[50] D. A. Kessler, H. Levine, and Y. Tu, Phys. Rev. A **43**, 4551 (1991).
[51] H. Leschhorn and L.-H. Tang, Phys. Rev. Lett. **70**, 2973 (1993).

Supporting Information for "Spatio-temporal patterns in ultra-slow domain wall creep dynamics"

Ezequiel E. Ferrero, Laura Foini, Thierry Giamarchi, Alejandro B. Kolton, Alberto Rosso

ABSTRACT

In this Supporting Information we present results that are both complementary and supplementary to the ones presented in the main text. We provide all the details about our model and its numerical implementation needed to reproduce our results. We also describe the different relevant length scales and universal exponents involved in the creep dynamics, presenting numerical results for different universality classes. These results further support the phenomenology described in the main text and also serves as a practical reference to translate our predictions to different physical systems. In particular, we show the events/clusters size distributions for the Random Field disorder case and consider the effect of a hard constraint or anharmonic corrections to the elasticity of the interface. Qualitative and quantitative predictions for a concrete experimental system are also presented.

A. ALGORITHMIC DETAILS

Our algorithm computes the irreversible dynamics below the depinning threshold of a one-dimensional elastic string uniformly driven in a two-dimensional discrete lattice in the low temperature limit.

The string is described by a discrete polymer with L elastically coupled monomers characterized at positions $h(i)$ $(i = 0, \dots, L-1)$. The string is coupled to a disordered potential $V(h(i), i)$ and to a uniform transverse driving force f. The system energy is given by:

$$E = \sum_i \frac{c}{2}(h(i+1) - h(i))^2 - fh(i) + V(i, h(i)). \quad \text{(S1)}$$

The Hooke springs between nearest neighbor monomers model an interface with short-range harmonic elasticity (we use $c = 2$). Besides this elastic energy, which preserves the statistical tilt symmetry (STS), we consider a numerically convenient hard metric constraint

$$|h(i) - h(i-1)| \leq 1, \quad \text{(S2)}$$

which significantly reduces the configuration space but violates STS (see an specific section below in this SI for a relevant discussion). We consider periodic boundary conditions in the longitudinal direction $h(L) \equiv h(0)$. The disorder matrix $V(h(i), i)$ is computed from uncorrelated Gaussian numbers $R_{j,i}$ with zero mean and unit variance, i.e. $\overline{R_{j,i}R_{j',i'}} = \delta_{i,i'}\delta_{j,j'}$, $\overline{R_{j,i}} = 1 - \overline{R_{j,i}^2} = 0$. To model the Random-Bond (RB) disorder we define $V_{RB}(h, i) = R_{h,i}$ such that $\overline{V_{RB}(j, i)V_{RB}(j', i')} = \delta_{i,i'}\delta_{j,j'}$, while for modeling the Random-Field (RF) disorder we define $V_{RF}(h, i) = \sum_{k=0}^{h} R_{k,i}$, such that $\overline{[V_{RF}(j, i) - V_{RF}(j', i')]^2} = \delta_{i,i'}|j - j'|$. In contrast to previous works where a periodicity in the transversal direction was considered for the disordered potential [16, 42] $(V(h(i), i) = V(h(i) + M, i))$ with M large enough, here we assume M to be infinite for all practical purposes.

As explained in the main text, the creep dynamics in the $T \to 0$ limit is described by performing movements that we call "creep events", which connect an ordered sequence of metastable states. Each of these events is composed of a thermally activated jump followed by a deterministic relaxation; both contributions make the string move in the forward direction.

The polymer position updates are performed as follows:

1. Starting from any blocked state (i.e., an energy local minimum) we find the smallest compact rearrangement that decreases the energy. This is, the smallest segment of the line such that by changing the position of its monomers to forward sites we obtain a lower global energy for the system. To this end we use the transfer matrix method locally, gradually decreasing the number of fixed (immobile) monomers until we find the desired move. This rearrangement implies jumping an energetic barrier.

2. After the above activated move, the string is not necessarily in a new energy minimum; so we let the line relax deterministically with the variant Monte Carlo technique [16]: The polymer follows the energy gradient by performing *elementary moves* consisting in collective one-site-forward increments of k consecutive monomers, with $k \in [1, L]$. When there is no further possible forward motion by deterministic relaxation, the line sits in a new blocked configuration, a new metastable state.

   The dynamics then retakes step 1 to find the next creep event.

The difference between the new and the previous metastable configurations is a compact object, well char-

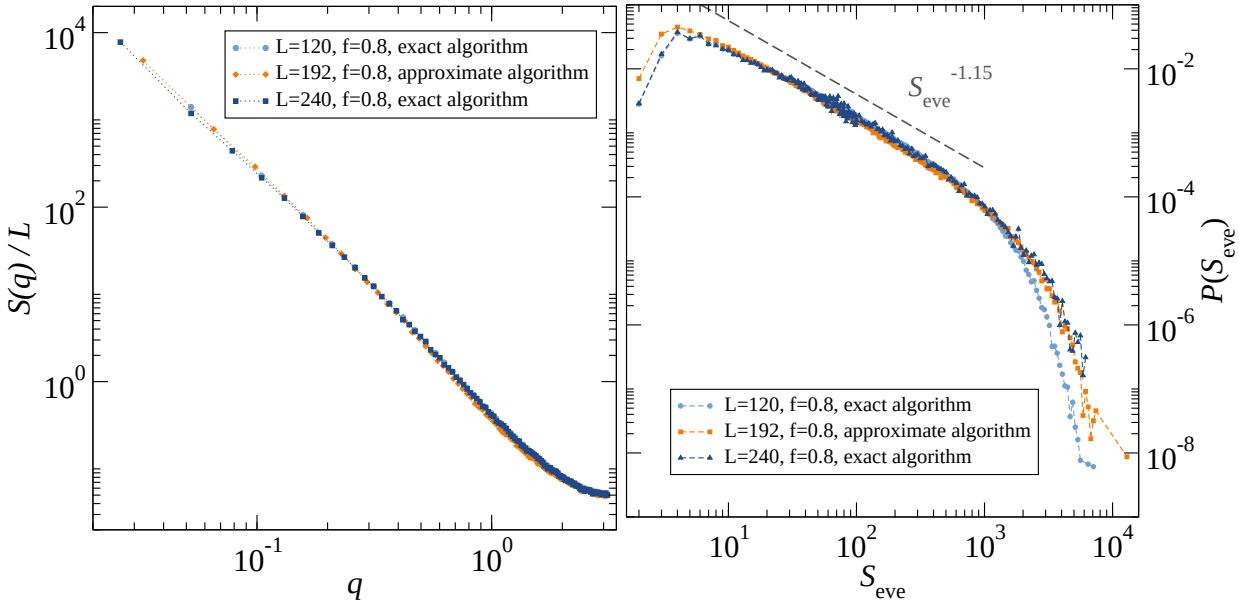

FIG. S1: *Left:* Average structure factors in the steady-state creep motion at $f = 0.8$. We compare the structure factor obtained with the approximate algorithm for $L = 192$, with the ones obtained with the exact algorithm for $L = 120, 240$. *Right:* Comparison of the creep event size distribution obtained with the exact and approximate algorithms for a driving force $f = 0.8$. The power law $P(S_{\rm eve}) \sim S_{\rm eve}^{-1.15}$ is shown as a guide to the eye.

acterized both by its area $S_{\rm eve}$ and by its lateral size $L_{\rm eve}$ (equal to the number of monomers involved in the jump). Our dynamics leads typically to a large sequence of creep events whose statistics we study in detail. For a given realization of the disorder, the sequence of metastable configurations generated with our algorithm is unique once the steady-state is reached. Typical sequences of blocked configurations can be seen in Fig.1 of the main text.

A. Approximation based on barriers scaling assumption

Our algorithm follows the same principles of the exact transition pathway algorithm explained in Refs. [16, 42] and it explores a sequence of metastable states associated with the low-T limit without solving a dynamical equation. Nevertheless, in step 1 above we have introduced a simplification, which makes it approximate: Instead of calculating explicitly the exact pathway connecting two consecutive metastable states through the *minimal energy barrier*, we target a new state by choosing the *smallest compact movement* that decreases the global energy. This approximation allow us to overcome the severe computational limitations the exact algorithm suffers at low forces at the expense of loosing access to the the actual energy barrier values and therefore to the real time.

In order to appreciate the differences between the exact transition pathways algorithm and the one used in this work, in Fig.S1-left and S1-right we compare, respectively, the average structure factor and the event size distribution at a given force. A statistical difference can only be appreciated for small events (small length scales and large wave-vectors q), presumably because of disregarding the existence of large energy barriers for some of the small rearrangements. In general the equivalence between the scaling of rearrangement sizes and energy barriers seems to work very well. Most importantly, differences at large scales, the ones that dominate the universal behavior we aim to study, are unobservable.

B. Parallel implementation on GPUs

Both step 1 and step 2 of the algorithm above are implemented in CUDA C to run in Graphic Processing Units used as a multipurpose hardware. We describe here only the most salient features of such an implementation.

In step 1 a thorough search of local moves should be accomplished and their potential energetic gain evaluated. We start by searching moves with $L_{\rm opt} = 1$ and increase $L_{\rm opt}$ progressively while no energetically favorable thermal nucleus is find. When looking for a partial move of size $L_{\rm opt}$ (that would leave unchanged the rest of the line) there are L possible starting points for the search, L discrete positions in the line. At that point is where we exploit the parallelism. A first CUDA kernel computes, for each starting point $(x_i, h(x_i))$ with $i \in [0, L-1]$, the current local energy of the line on an extension $L_{\rm opt}$ in a predefined direction and observing the periodic boundary conditions. A second CUDA kernel performs the transfer matrix forward branch of the search for each start-

ing point $(x_i, h(x_i))$ on an extension $L_{\rm opt}$ and fix ending point at $(\lfloor x_i + L_{\rm opt} \rfloor_L, h(\lfloor x_i + L_{\rm opt} \rfloor_L)$, choosing the best option for a newly proposed local configuration. This is, it selects a new local configuration that would produce the most favorable energetic change given the constraints (fix points, had-constraint, p.b.c.). After that, combined parallel primitives of the Thrust library are used to compare the local energies of the current and proposed configurations and choose the one that gives the maximum energetic gain, if any. If at least one of the L proposed moves decrease the energy, the single chosen one is performed by a couple of CUDA kernels that perform the full transfer matrix move (forward and backward branches) updating the line configuration to its new position, and the algorithm moves to step 2. If not, $L_{\rm opt}$ is increased in one unit and the search relaunched.

The deterministic relaxation of step 2 also profits from the massive parallelism of GPUs. It follows the (zero temperature) Variational Monte Carlo procedure explained in [16, 43]. There, we attempt to move *one step forward* a compact block of k monomers at no energetic cost, i.e., accepting the move only if it decreases or lets unchanged the energy of the system. This is called an "elementary move" of size k. We start looking for elementary moves with $k = 1$ and progressively increase k by one unit when all the moves for the current k value have been exhausted. Only one elementary move is performed at a time, but L of them are proposed and evaluated in parallel by a CUDA kernel. A Thurst parallel find primitive helps to locate the first favorable elementary move in a sequence identified by its starting point, and this one is performed by a simple update kernel. Whenever an elementary move is performed for $k > 1$, the search restarts from $k = 1$. Step 2 of our creep algorithm finishes when k reaches the system size L, or alternatively, a computationally convenient maximum given value K_{max} set to be large enough to contemplate even the biggest elementary moves observed in trial runs with unbounded k for each force.

Besides the two-step algorithm for the creep dynamics, which is at the core of our implementation, parallelism is also exploited for computing different observables. Examples are the subtraction of two consecutive metastable configurations to get $L_{\rm eve}, S_{\rm eve}$, made by proper Thrust transformation and reduction; or the computation of the structure factor $S(q)$, made using the CUFFT parallel fast Fourier transform library.

Our codes will be freely available to the community upon request.

B. RELEVANT EXPONENTS FOR THE CREEP DESCRIPTION

Being an intermediate regime between two fixed points of the dynamics [24], the creep is described by both equilibrium and depinning exponents [16, 42], rather than by different ones.

1d RB exponents	**estimate**	**Figure**
$\zeta_{\rm eq}$	2/3	3-right
$\nu_{\rm eq} = 1/(2-\zeta_{\rm eq})$	3/4	3-left, S3-left
$\tau_{\rm eq} = 2 - 2/(1+\zeta_{\rm eq})$	4/5	4-left
$\theta_{\rm eq} = 2\zeta_{\rm eq} - 1$	1/3	–
$\mu = \theta_{\rm eq}\nu_{\rm eq}$	1/4	–
1d RF exponents	**estimate**	**Figure**
$\zeta_{\rm eq}^{\rm RF}$	1	S4
$\nu_{\rm eq}^{\rm RF} = 1/(2-\zeta_{\rm eq}^{\rm RF})$	1	S3-left
$\tau_{\rm eq}^{\rm RF} = 2 - 2/(1+\zeta_{\rm eq}^{\rm RF})$	1	S7-left
$\theta_{\rm eq}^{RF} = 2\zeta_{\rm eq}^{\rm RF} - 1$	1	–
$\mu^{\rm RF} = \theta_{\rm eq}^{RF}\nu_{\rm eq}^{\rm RF}$	1	–
1d RB & RF exponents	**estimate**	**Figure**
$\zeta_{\rm dep}$	1.250	3-right, S4
$\nu_{\rm dep} = 1/(2-\zeta_{\rm dep})$	1.333	–
$\tau_{\rm dep} = 2 - 2/(1+\zeta_{\rm dep})$	1.11	4-left, S7-left
$\zeta_{\rm dep}^{\rm anh}$	0.65	S4, S6-left
$\nu_{\rm dep}^{\rm anh}$	1.75	–
$\tau_{\rm dep}^{\rm anh} = 2 - (1/\nu_{\rm dep}^{\rm anh} + \zeta_{\rm dep}^{\rm anh})/(1+\zeta_{\rm dep}^{\rm anh})$	1.25	S6-right

TABLE S1: Universal exponents relevant for the one dimensional creep motion, for short range elastic interactions in presence of a hard-constraint, according to the disorder type.

In Table S1 we list the numerical estimates observed for the universal exponents characterizing the creep motion of a one dimensional elastic line for RF and RB disorders, in presence of the metric constraint of Eq.S2. The numerically observed roughness exponents agree well with previous estimates: at equilibrium $\zeta_{\rm eq} = 2/3$ [35], $\zeta_{\rm eq}^{\rm RF} = 1$ [44, 45], and at depinning, $\zeta_{\rm dep} \approx 1.25$ [39, 45, 46], $\zeta_{\rm dep}^{\rm anh} \approx 0.63$[16, 47]. As indicated, the corresponding exponents $\nu_{\rm dep}, \nu_{\rm eq}, \nu_{\rm eq}^{\rm RF}$ can be estimated exploiting the statistical tilt symmetry (STS) relation, $\nu = 1/(2-\zeta)$, except for $\nu_{\rm dep}^{\rm anh}$, corresponding to the anharmonic non-STS case. The observed avalanche size exponents, $\tau_{\rm eq}, \tau_{\rm eq}^{\rm RF}, \tau_{\rm dep}$, agree well with the Narayan-Fisher (NF) conjecture [29], $\tau = 2 - 2/(1+\zeta)$ with $\zeta = \zeta_{\rm eq}, \zeta_{\rm eq}^{\rm RF}, \zeta_{\rm dep}$ respectively. On the other hand, in the anharmonic elasticity case, where STS is violated, the avalanche exponent $\tau_{\rm dep}^{\rm anh}$ agrees fairly with the generalized form of the NF conjecture $\tau = 2 - (1/\nu + \zeta)/(1+\zeta)$ (see Supplementary Information in [48]) using the value $\nu_{\rm dep}^{\rm anh} \approx 1.75$ extracted from Ref.[7].

It is worth remarking that exponents for RB and RF are identical at large length-scales where depinning dominates, since RB and RF share a unique depinning universality class. At intermediate scales, where equilibrium dominates instead, exponents are different among RB and RF disorder, since they belong to different equilibrium universality classes.

C. CHARACTERISTIC LENGTH SCALES

Spatio-temporal patterns in creep dynamics are controlled by a few characteristic static and dynamic length-scales. They describe different geometrical regimes of roughness and the characteristic sizes of individual or cluster of events. We describe them in this section, going from the shortest non-universal length-scale, to the largest scales, displaying universal dynamical behavior.

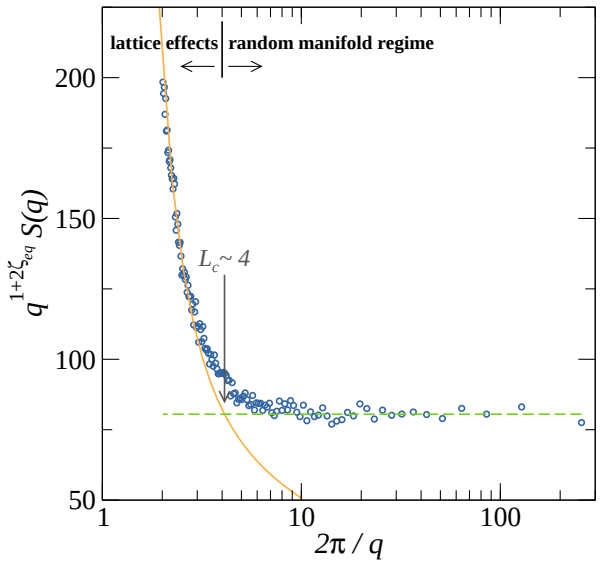

FIG. S2: Effective Larkin length L_c obtained from the crossover to the random-manifold in the ground-state ($f = 0$) geometry of a $L = 256$ system for RB disorder. At short length-scales the purely thermal discrete correlator $S_q \sim [2\sin(q/2)]^{-2}$ fits well the large q regime showing that below L_c non-universal lattice effects are relevant. Above L_c the geometry is universal and well described by $S_q \sim 1/q^{1+2\zeta_{\rm eq}}$ with $\zeta_{\rm eq} = 2/3$ the equilibrium roughness. Indistinguishable values for L_c for different steady-state configurations in the $0 < f \leq f_c$ creep regime are found.

A. Effective Larkin length

Similarly to the continuum model [49], in the lattice model we can define an *effective Larkin length* $L_{\rm c}$ as the crossover length separating a non-universal microscopic regime (determined by the details of the lattice model) from the universal "random manifold" regimes that emerge at larger length scales.

To fix ideas, let $w(L) \equiv \sqrt{\sum_i [h(i) - h_{cm}]^2 / L}$ (with $h_{cm} = \sum_i h(i)/L$) be the width or roughness of an interface of size L. At the fix points of equilibrium and depinning, the string has a self-affine structure with a well defined exponent ζ (equal to $\zeta_{\rm eq}$ and $\zeta_{\rm dep}$ respectively). In those cases, for the global roughness we can write, when $L \gg L_{\rm c}$,

$$w(L) \approx w_c \left(\frac{L}{L_{\rm c}}\right)^{\zeta}, \tag{S3}$$

with w_c being the characteristic width at the scale $L_{\rm c}$. Alternatively, one can write for such state the structure factor,

$$S_q \approx q^{-(1+2\zeta)} G(qL_{\rm c}), \tag{S4}$$

with $G(x) \sim cte$ for $x \ll 1$, and for $x > 1$ $G(x)$ describes the microscopic behaviour, affected by microscopic details such as discreteness and the finite disorder correlation length.

In Fig.S2 we determine $L_{\rm c}$ for the equilibrium structure factor, using the same parameters as in our creep simulations. We obtain the rough estimate $L_{\rm c} \approx 4$ from the crossing of the two asymptotic forms of S_q: we find that the large q behavior is well described by the purely thermal discrete correlator $S_q \sim [2\sin(q/2)]^{-2}$, while the small q behavior clearly displays self-affine scaling with the known exponent $\zeta_{\rm eq} = 2/3$. Similar values of $L_{\rm c}$ are obtained for the RF ground state (with $\zeta_{\rm eq} \approx 1$), for the critical depinning state (with roughness exponent $\zeta_{\rm dep} \approx 1.25$), and also for metastable creep states. In all cases, we find that $w_c \approx r_f$, as expected from the Larkin estimate for the continuum model, with the correlation length of the random force set to $r_f = 1$ (see disorder definition in the *Algorithmic details* section).

As in the continuous case, $L_{\rm c}$ depends on the strengths of the elasticity and of the disorder. Most importantly, the value for $L_{\rm c}$ estimated can be used as the unit of length to express quantitatively large scale universal properties for a system with particular microscopic details. For instance the creep length for $f \to 0$ should behave as $L_{\rm opt} \approx L_{\rm c}(f/f_c)^{-\nu_{\rm eq}}$, with f_c the critical depinning force. For our simulations in the RB case the sample averaged critical depinning force obtained with the same variant Monte Carlo technique used in Ref. [39] gives $f_c \approx 1.2$. We thus predict $L_{\rm opt} \approx 4.6 f^{-\nu_{\rm eq}}$ in excellent quantitative agreement with the crossover from equilibrium ($\zeta_{\rm eq}$) to depinning roughness ($\zeta_{\rm dep}$) at wave-vector $q_{\rm opt} \approx 1.4 f^{\nu_{\rm eq}}$, shown in of Fig.4-right of the main text: using that $2\pi/q_{\rm opt} \approx 4.5 f^{-\nu_{\rm eq}}$ we conclude that $L_{\rm opt} \equiv 2\pi/q_{\rm opt} \approx L_{\rm c}(f/f_c)^{-\nu_{\rm eq}}$.

B. Dynamical Lengths

A single event separating two metastable states in the creep regime has a typical lateral size $L_{\rm eve}$ and and area $S_{\rm eve}$. It is composed of an activated part, with a characteristic lateral size $L_{\rm opt}$ and area $S_{\rm opt} \approx w_c L_c (L_{\rm opt}/L_{\rm c})^{\zeta_{\rm eq}+1}$. The subsequent deterministic relaxation towards the next metastable state yields a total characteristic size $L_{\rm eve} \geq L_{\rm opt}$ and $S_{\rm eve} \sim L_{\rm eve} \times L_{\rm opt}^{\zeta_{\rm eq}} (L_{\rm eve}/L_{\rm opt})^{\zeta_{\rm dep}} > S_{\rm opt}$. These steady-state dynamical lengths controlling creep motion are driving-force

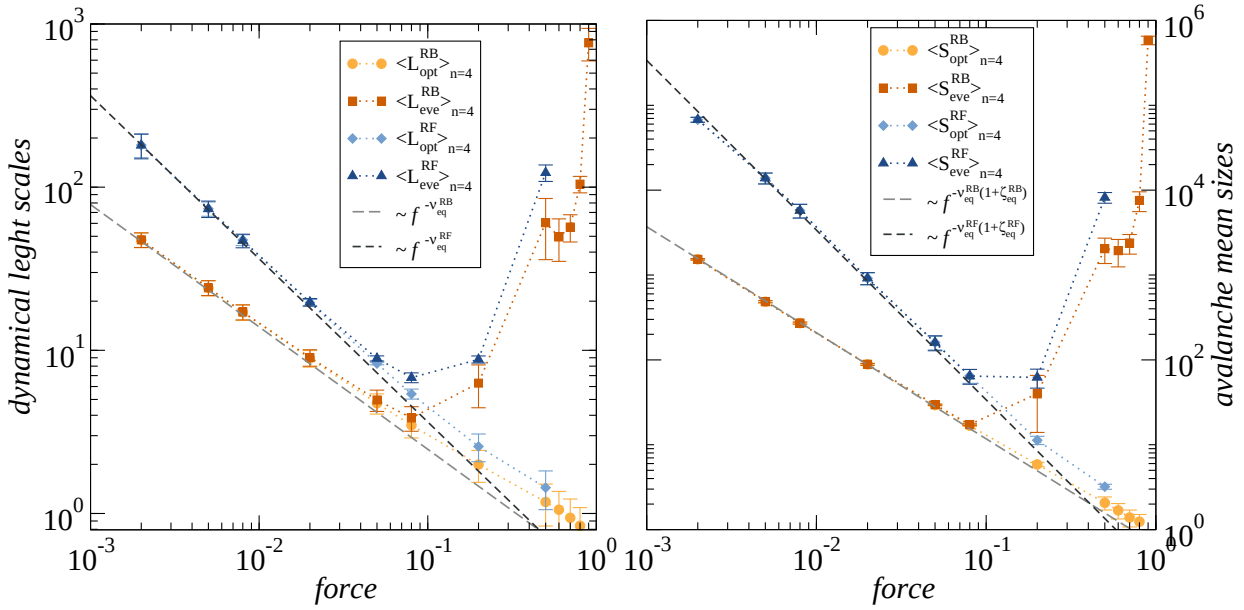

FIG. S3: *Left:* Dynamical lengths in the creep regime for Random-Bond and Random-Field disorders. A creep event is composed by an activated part of characteristic lateral size $L_{\rm opt}$, followed by a deterministic relaxation adding to a total characteristic lateral size $L_{\rm eve}$. Divergent behaviors appear at the characteristic forces $f = 0$ (ground-state), where $L_{\rm opt}$ diverges, and at $f = f_c$, where $L_{\rm eve}$ diverges. These divergences are controlled by equilibrium and depinning exponents respectively. Dashed lines show the universal power-law divergence expected as $f \to 0$ from the phenomenological creep theory. *Right:* Mean avalanche sizes (areas) of creep events for Random-Bond and Random-Field disorders. The activated part of the event has a characteristic area $S_{\rm opt} \sim L_{\rm opt}^{\zeta+1}$. Deterministic relaxation makes the activated event grow up to a characteristic area $S_{\rm eve} \sim L_{\rm eve}^{\zeta_{\rm dep}+1}$. Divergent behaviors arise from the divergence of the characteristic lengths, $L_{\rm opt} \xrightarrow[f\to 0]{} \infty$, $L_{\rm eve} \xrightarrow[f\to f_c^-]{} \infty$. Dashed lines show the universal power-law divergence expected as $f \to 0$ from the phenomenological creep theory. In each case the mean value of fourth order $\langle X\rangle_{n=4} = \langle X^4\rangle / (3\langle X^3\rangle)$ is shown. The error bars are estimated from the difference with the values given by $\langle X\rangle_{n=3}$. Data correspond to simulations of a system size $L = 3360$.

dependent. In Fig. S3-left we show that at low forces $L_{\rm opt} \sim f^{-\nu_{\rm eq}}$, with $\nu_{\rm eq} = 1/(2-\zeta_{\rm eq}^{\rm RB}) = 3/4$ for RB disorder and $\nu_{\rm eq} = 1/(2-\zeta_{\rm eq}^{\rm RF}) = 1$ for RF disorder, as predicted by the phenomenological creep theory.

This behavior of $L_{\rm opt}$ explains the scaling at low forces shown in Fig.S3-right, since $S_{\rm opt} \sim L_{\rm opt}^{\zeta_{\rm eq}+1} \sim f^{-\nu_{\rm eq}(\zeta_{\rm eq}+1)} \sim f^{-5/4}$ for RB disorder ($S_{\rm opt} \sim f^{-2}$ for RF disorder). Notice that in order to catch systematically ($L_{\rm opt}$,$S_{\rm opt}$, $L_{\rm eve}$,$S_{\rm eve}$) as the length/size scales characterizing the cutoffs of distributions that we do not inspect individually, we have taken a combination of higher order moments instead of simply the averages (see Fig.S3 caption).

Noteworthy, the characteristic size of a creep event is also a geometrical crossover length between $\zeta_{\rm eq}$ and $\zeta_{\rm dep}$, as demonstrated by the rescaled structure factors in Fig.S4, for RB and RB disorders. In figures S3-left and S3-right we also show that at forces close to the critical force $L_{\rm eve}$ and $S_{\rm eve}$ tend to diverge. In this case, it is the deterministic relaxation part that dominates the dynamics, consistent with the subthreshold behavior $L_{\rm eve} \sim (f_c - f)^{-\nu_{\rm dep}}$ reported in Ref. [16, 42]. Our results extend however the analysis made in Ref. [16, 42] to the regime of low forces where simple creep scaling holds, validating some phenomenological predictions made 30 years ago [20, 21].

C. Hard Constraint induced crossover length

For small driving forces, the large scale roughness exponent $\zeta_{\rm dep} \approx 1.25$ was obtained *directly* from the structure factor by fitting $S_q \sim 1/q^{1+2\zeta_{\rm dep}}$ in Fig. S4 at large lengthscales $q \ll 1$. This value is consistent with Fig.4-left in the main text, which shows a good agreement with the expression $\tau = 2 - 2/(1+\zeta_{\rm dep})$, expected for depinning avalanches. On the other hand, the value of $\zeta_{\rm dep}$ is indistinguishable from the roughness exponent of critical configurations at $f = f_c$ in the quenched Edwards-Wilkinson universality class (QEW), accurately obtained both for continuum models and in particular for the discrete model with the energy of Eq.S1. If the constraint of Eq.S2 is present, however, the roughness exponent

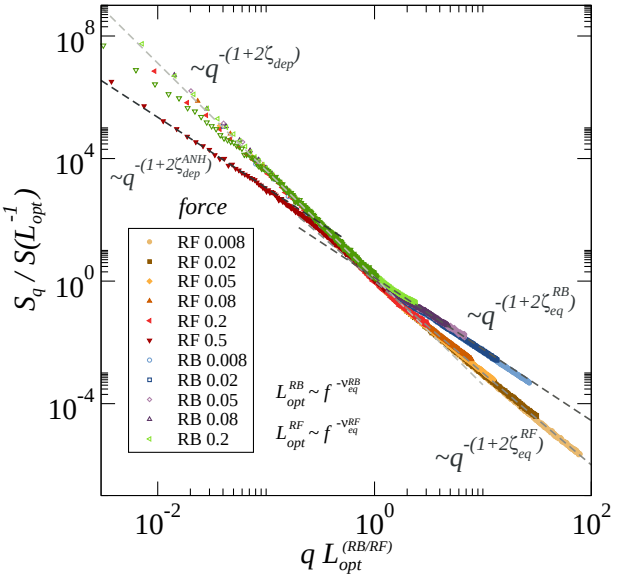

FIG. S4: Rescaled structure factor for Random Field and Random Bond disorders. Curves correspond to forces $f = \{0.008, 0.02, 0.05, 0.08, 0.2, 0.5\}$, for a fixed system size $L = 3360$. At large length-scales the geometry is described in both cases by the harmonic depinning roughness exponent $\zeta_{\rm dep} \approx 1.25$ (except for the larger forces that already display the crossover to anharmonic depinning $\zeta_{\rm dep}^{\rm anh} \approx 0.65$), while below the characteristic (disorder dependent) crossover length $L_{\rm opt} \sim f^{-\nu_{\rm eq}}$, the equilibrium roughness $\zeta_{\rm eq}$ is different for RB and RF disorders since ${\zeta_{\rm eq}}^{RB} = 2/3$ and ${\zeta_{\rm eq}}^{RF} = 1$. Short non-universal length-scales $q > 2\pi/L_c$ with $L_{\rm c} \sim 10$ were removed from all curves.

$\zeta_{\rm dep}^{\rm anh} \approx 0.63$ is expected both for continuum [47] or lattice models [16], at $f = f_c$ or in the creep regime $f < f_c$. Moreover, a whole family of anharmonic corrections to the elasticity [39, 47] drive the depinning from QEW to quenched Kardar-Parisi-Zhang (QKPZ) universality class [50]. We need then to understand why in our simulations at low drives we only observe $\zeta_{\rm dep} \approx 1.25$ instead of $\zeta_{\rm dep}^{\rm anh} \approx 0.63$, in spite of imposing Eq.S2.

In this section we show that deep in the creep regime, Eq.S2 yields results that are compatible with the purely harmonic model because of the existence and rapid growth of a crossover length from harmonic to anharmonic elastic behavior as the driving force decreases. To get a rough estimate, the hard constraint is expected to be relevant when the global width is $w(\ell) > \ell$ and hence a finite fraction of local displacements reach the hard-constraint wall of Eq.S2. We can then expect a crossover from harmonic to anharmonic roughness at the length scale $L_{\rm anh}$, such that

$$w(L_{\rm anh}) \approx L_{\rm anh} \tag{S5}$$

Deep in the creep regime, in the low temperature limit, the width of interfaces at different length scales $\ell < L_{\rm anh}$ (see dynamical crossover diagram of Ref.[16]) can be written as

$$w(\ell) \approx \begin{cases} w_c \left(\frac{\ell}{L_{\rm c}}\right)^{\zeta_{\rm eq}}, & \text{if } L_{\rm c} < \ell < L_{\rm opt} \\ w_c \left(\frac{L_{\rm opt}}{L_{\rm c}}\right)^{\zeta_{\rm eq}} \left(\frac{\ell}{L_{\rm opt}}\right)^{\zeta_{\rm dep}}, & \text{if } L_{\rm opt} < \ell < L_{\rm anh} \end{cases}, \tag{S6}$$

where w_c is the effective width at $L_{\rm c}$. To write the above equation we are making three assumptions: (i) The crossovers between the roughness regimes are sharp enough to make them match at the characteristic crossover lengths; (ii) Since $\zeta_{\rm eq} = 2/3$ and typically $w_c/{L_{\rm c}}^{\zeta_{\rm eq}} < 1$ (valid when the disorder is not extremely strong), the crossover to the anharmonic regime will occur in the depinning roughness regime, since in such regime the average local elongation $w(\ell)/\ell$ grows with the observation length, due to the inequality $\zeta_{\rm dep} > 1$ [51]. (iii) We are also assuming that $L_{\rm anh} < L_{\rm av}$, with $L_{\rm av}$ the crossover length to the fast-flow regime of roughness [27]. This is justified, since $L_{\rm av}$ diverges when the velocity vanishes (our $T \to 0+$ creep simulations strictly correspond to this limit). Under these assumptions, well met in our study, and using Eqs. S5 and S6 we finally get an estimate of the harmonic to anharmonic elasticity crossover length

$$L_{\rm anh} \approx \left({L_{\rm c}}^{\zeta_{\rm eq}}/w_c\right)^{\frac{1}{\zeta_{\rm dep}-1}} L_{\rm opt}^{\frac{\zeta_{\rm dep}-\zeta_{\rm eq}}{\zeta_{\rm dep}-1}}. \tag{S7}$$

For $L_{\rm anh} < \ell$ we thus expect an anharmonic regime of roughness

$$w(\ell) \approx L_{\rm anh} \left(\frac{\ell}{L_{\rm anh}}\right)^{\zeta_{\rm dep}^{\rm anh}}. \tag{S8}$$

with $\zeta_{\rm dep}^{\rm anh} \approx 0.63$. In Fig.S5 we show schematically the theoretically expected geometrical crossover diagram and Fig.S4 already shows this crossover in the structure factor for large enough forces. We estimate from S_q and exponent $\zeta_{\rm dep}^{\rm anh} \sim 0.65$, very close to previous estimations [16].

Let us now make quantitative estimates and compare with our simulations. For the RB disorder we have $\zeta_{\rm eq} = 2/3$ and $\zeta_{\rm dep} \approx 5/4$. We thus get from Eq.S7

$$L_{\rm anh} \approx L_c \left(L_c/w_c\right)^4 \left(L_{\rm opt}/L_{\rm c}\right)^{7/3} \tag{S9}$$

In Fig.S6-left we show that this scaling works fairly well, by using that near the crossover at $L_{\rm anh}$, $S_q \sim q^{-(1+2\zeta_{\rm dep}^{\rm anh})} H(qL_{\rm anh})$ with $H(x) \sim x^{\zeta_{\rm dep}^{\rm anh}-\zeta_{\rm dep}}$ for $x > 1$ and $H(x) \sim$ const for $x < 1$. For forces $f \lesssim f_c$ the observation of the anharmonic regime in a finite system thus depends on the value ${L_{\rm c}}^{\zeta_{\rm eq}}/w_c$. For our case, we get $({L_{\rm c}}^{2/3}/w_c)^4 \approx 40$. Using that $L_{\rm opt} \approx 4.5 f^{-3/4}$ (see Fig.4-right in the main text) we get $L_{\rm anh} \approx 180\ f^{-7/4}$. The anharmonic regime hence should become unobservable for forces $f < (L/180)^{-4/7}$, in very good agreement with Fig. S6-left for $L = 3360$. It is worth noting that for larger forces however, the anharmonic effects

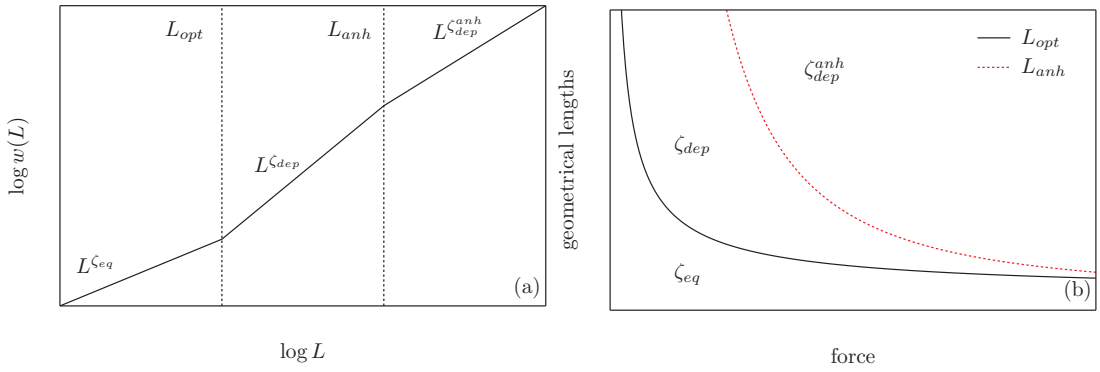

FIG. S5: (a) Scheme of the interface global width with its size in the creep regime, showing the dynamical crossover lenght $L_{\rm opt}$ from $\zeta_{\rm eq}$ to $\zeta_{\rm dep}$, and the crossover lenght $L_{\rm anh}$ from $\zeta_{\rm dep}$ to $\zeta^{\rm anh}_{\rm dep}$ produced by the hard constraint Eq.S2. (b) $L_{\rm anh}$ is expected to grow quickly with $L_{\rm opt}$.

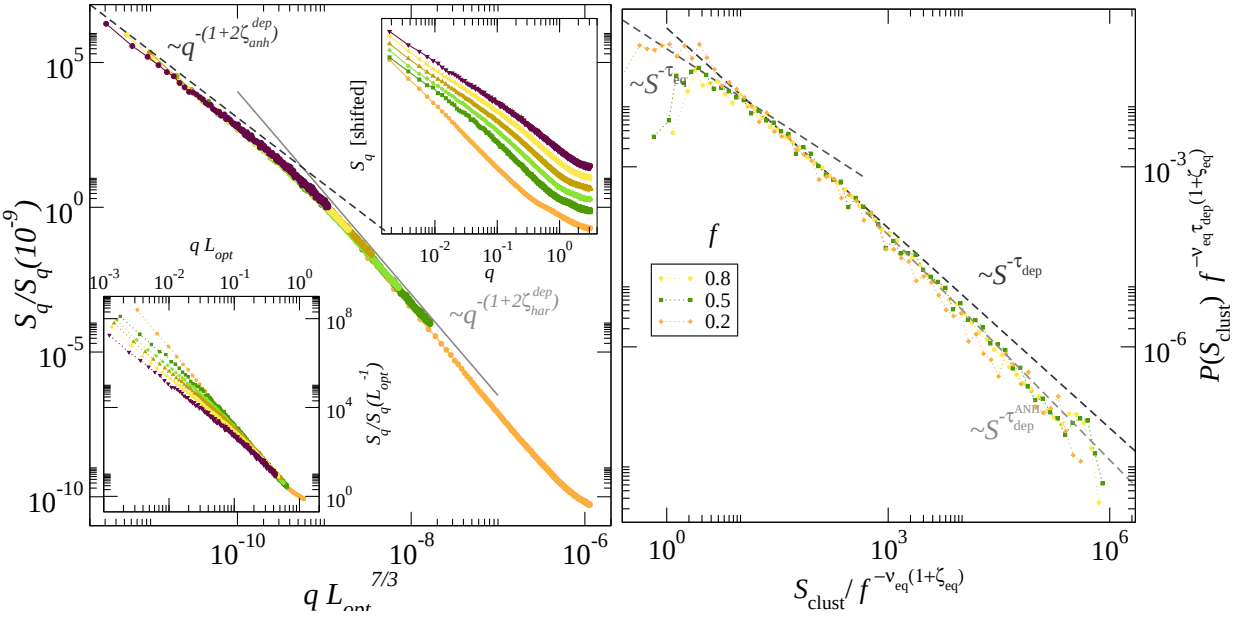

FIG. S6: *Left*: Structure factor for the Random Bond case showing the characteristic lengthscale $L_{\rm anh}$ which separate the harmonic depinning regime with roughness exponent $\zeta_{\rm dep}$ from the anharmonic depinning regime with exponent $\zeta^{\rm anh}_{\rm dep}$, for different high forces $f \in \{0.2, 0.5, 0.6, 0.7, 0.8, 0.9\}$, $L = 3360$. The upper-right inset shows the raw structure factor arbitrarily shifted in the vertical direction for different forces for a better display. The bottom-left plot shows S_q scaled with $L_{\rm opt}$ as in Fig.4-right of the maintext. The main panel shows the structure factor rescaled with $L_{\rm anh} \propto (L_{\rm opt}/L_{\rm c})^{7/3}$, as proposed in Eq.S9. Straight gray lines are a guide to the eye, showing slopes corresponding to $\zeta_{\rm dep} \simeq 1.25$ (full line) and $\zeta^{\rm anh}_{\rm dep} \simeq 0.65$ (dash line). *Right*: Cluster size distributions for $L = 3360$ and $f \in \{0.2, 0.5, 0.8\}$. The anharmonic crossover has consequences in the cluster distribution for large cluster sizes. In the depinning regime the power law decay has a crossover from a regime described by $\tau_{\rm dep} \approx 1.11$ to a regime described by $\tau^{\rm anh}_{\rm dep} \approx 1.25$ indicated by the two dashed lines.

are visible both in S_q, where the exponent $\zeta^{\rm anh}_{\rm dep}$ appears, and also in the cluster size distribution at large sizes, shown in Fig. S6-right, where the decay exponent is very close to the one expected in the QKPZ universality class, $\tau^{\rm anh}_{\rm dep} = 2 - (1/\nu^{\rm anh}_{\rm dep} + \zeta^{\rm anh}_{\rm dep})/(1 + \zeta^{\rm anh}_{\rm dep}) \approx 1.25$. (general relations where derived in Ref.[48]).

The same analysis for the RF disorder where $\zeta_{\rm eq} = 1$ [44] and $\zeta_{\rm dep} \approx 5/4$ [39], gives

$$L_{\rm anh} \approx (L_{\rm c}/w_c)^4\, L_{\rm opt}, \qquad \text{(S10)}$$

so anharmonic effects are expected to be stronger in the RF case (as can be seen in Fig.S4 comparing RB and RF

for the same force).

In summary, the above analysis shows that deep in the creep regime the effects of Eq.S2 appear only at very large scales compared to $L_{\rm opt}$, for both RB and RF disorder. They are thus irrelevant in the $f \to 0$ limit, supporting our interpretation of large clusters of correlated activated events as depinning-like avalanches in the QEW universality class, rather than in the QKPZ universality class. It is worth noting however, that the argument made for $L_{\rm anh}$ remains valid whenever the harmonic elasticity breaks down at $w(L_{\rm anh}) \sim aL_{\rm anh}$, with a some constant, to a harder, softer, or even plastic regime. The QEW class may be thus *physically relevant*, i.e. experimentally suitable, in spite of predicting a depinning roughness $\zeta_{\rm dep} > 1$ (in $d = 1$) which is asymptotically incompatible with the harmonic elastic approximation [51]. This might explain why magnetic domain wall dynamics experiments display effective exponents which are close to those of the QEW class [34] (see discussion in section *Predictions for ultrathin Pt/Co/Pt magnetic films* below).

D. EVENT DISTRIBUTIONS FOR RF AND RB DISORDER

The fact that RB and RF disorders have the same depinning but different equilibrium exponents has visible consequences in the creep event distributions. In figure S7-right we show that the distribution of individual events decay faster for RF than for RB disorder. On the other hand in Fig. S7-left we show that the distribution of cluster sizes decays, for large sizes, as a power law with an exponent $\tau_{\rm dep} \approx 2 - 2/(1 + \zeta_{\rm dep}) \approx 10/9$ for RF disorder, in accordance with Fig.4-left and the fact that depinning exponents are identical for RB and RF. For sizes smaller that $L_{\rm opt}$ however, the RF cluster distribution in Fig. S7-left is better described by a power law decay with exponent $\tau_{\rm eq}^{\rm RF} \approx 2 - 2/(1 + \zeta_{\rm eq}^{\rm RF}) \approx 1$, even visually distinguishable from the exponent $\tau_{\rm eq} \approx 4/5$ of the RB case in Fig.4-left. For an exponents summary see Table S1.

E. FINITE SIZE EFFECTS

As mentioned in the main text, the upper cutoff for the cluster size distribution $P(S_{\rm clust})$ is set by the system size and not by an intrinsic physical mechanism. In the ideal case of the thermodynamic limit, the depinning scaling for $P(S_{\rm clust})$ should have no cutoff at all. Nevertheless, it is worth recalling that the imposition of a hard-constraint yields the appearance of a harmonic to anharmonic crossover in the depinning regime, so eventually, it would be the anharmonic depinning scaling the one with no cutoff in the thermodynamic limit.

It was also mentioned that our procedure to build clusters is affected by the existence of "percolating clusters", this is, by clusters whose lateral size reaches the system size L. In that case we start a new cluster with the next event. The occurrence of percolating clusters for a given force is evidently more frequent for smaller systems. This clusters accumulate at the tail of the distribution forming a "bump" that is clearly more prominent for smaller systems, as can be seen in Fig.S8. Even more, the finite system size acts as an absorbing boundary for the probability of $S_{\rm clust}$. If a cluster has grown to a lateral size $L_{\rm clust}$ comparable to L, there is no much space left for the appearance of an independent nucleus to start a new cluster, therefore the cluster may keep growing. This absorbing boundary effect can be clearly visualized in the gap formed before the bump for the smallest system size and smallest force in Fig.S8.

The second noticeable finite size effect is that, by controlling the frequency of percolating clusters, the system size also affects the sampling of the small clusters, i.e., the equilibrium regime. Surprisingly enough, a bigger rate of accumulation at the bump, also generates an over population of small clusters (typically happening after a percolating one). This clearly shifts the $P(S_{\rm clust})$ curves in the equilibrium regime, but as far as we can see, it does not affect the power law scaling, neither small clusters disappear as we get rid of finite size effects.

To conclude this section, let us mention that, in turn, the structure factor S_q shows no finite size effects, except from the trivial change of values of q accessed. As can be seen in the inset of Fig.S8, it always display quite clearly the crossover between a depinning regime and an equilibrium regime, at a length scale that does not depend on system size. Therefore reinforcing our previous considerations on the role of a finite system size.

F. PREDICTIONS FOR ULTRATHIN PT/CO/PT MAGNETIC FILMS

The experimental observations [1] of the creep exponent $\mu \approx 0.24 \pm 0.04$, the roughness exponent $\zeta \approx 0.69 \pm 0.07$, and the thermal rounding exponent [34] $\psi \approx 0.15 \pm 0.05$ in ultrathin Pt/Co/Pt magnetic films supports the hypothesis that, at the relevant length scales for creep motion, these domain walls belong to the universality class of one dimensional interfaces with short ranged elasticity and random bond disorder. We indeed expect [20, 21, 36] $\mu = (2\zeta_{\rm eq} - 1)/(2 - \zeta_{\rm eq}) = 1/4$, and [35] $\zeta_{\rm eq} = 2/3$ and [27] $\psi \approx 0.15$ for this class.

Recently, the field-driven domain wall dynamics in ultrathin Pt(0.35nm)/Co(0.45nm)/Pt(0.35nm) magnetic films with perpendicular anisotropy was studied by magneto-optical Kerr microscopy, from 50 K to 300 K [34]. By fitting the velocity force characteristics in the creep and depinning regimes, a critical depinning field $H_{\rm dep} \approx 1000$ Oe and a characteristic energy scale $T_{dep} \approx 2000\ K$ were obtained at room temperature ($T = 300\ K$). Using weak pinning theory the Larkin length was estimated as $L_c = (k_B T_{dep})/[(M_s H_{dep} t) w_c] \approx$

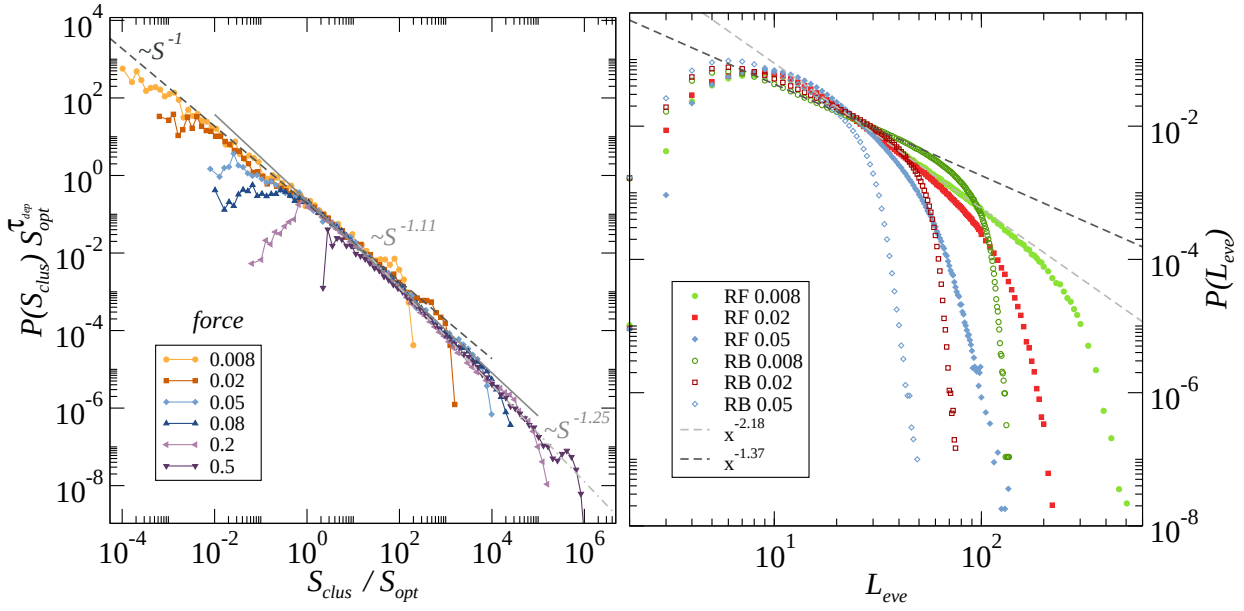

FIG. S7: *Left*: Cluster size distribution for Random Field disorder and different forces. As in the RB case, crossovers from equilibrium to harmonic depinning and then, from harmonic depinning to anharmonic depinning, are observed when we scale $S_{\rm clust}$ with $S_{\rm opt} \simeq f^{-\nu_{\rm eq}^{\rm RF}(1+\zeta_{\rm eq}^{\rm RF})}$. Notice that now, both the scaling size $S_{\rm opt}$ and the exponent of the equilibrium power-law regime ($\nu_{\rm eq}^{\rm RF} = 1$) have changed. *Right*: Comparison between the event size distribution for RB and RF disorder for three different driving forces. Dashed lines indicate fits to an effective non-universal power law decay at intermediate sizes. In general the curves for RF disorder decrease faster and have a later cutoff.

0.04 μm, where $w_c \approx 20\ \mu m$ is of the order of the domain wall width, $t \approx 0.45\ nm$ is the thickness of the sample and $M_s \approx 800\ erg/G.cm^3$ the saturation magnetization. This allows us to predict $L_{\rm opt}$ (Fig.4-right in the main text and Fig.S3-left) for this system,

$$L_{\rm opt} = L_{\rm c}(H_{dep}/H)^{\nu_{\rm eq}} \approx 40nm(H_{dep}/H)^{0.75}, \quad \text{(S11)}$$

$$h_{\rm opt} = w_c(L_{\rm opt}/L_{\rm c})^{\zeta_{\rm eq}} \approx 20nm(H_{dep}/H)^{0.5}. \quad \text{(S12)}$$

where $h_{\rm opt}$ is the displacement associated with $L_{\rm opt}$. Interestingly this implies that the two dimensional shape of creep events become increasingly compressed in the direction of motion as we reduce H, the aspect ratio scaling as $L_{\rm opt}/h_{\rm opt} \approx 2(H_{dep}/H)^{0.25}$. On the other hand, the area distribution cut-off of these events (as shown in Fig.3-left in the main text) is predicted to scale as

$$S_{\rm opt} = w_c L_c (L_{\rm opt}/L_{\rm c})^{\zeta_{\rm eq}+1} \approx 800\ nm^2 (H_{dep}/H)^{1.25} \quad \text{(S13)}$$

For a given field, detecting individual creep events of such sizes is mainly limited by the spatial resolution of the imaging technique. Using a spatial resolution of 1 μm, which is typical for magneto-optical setups, assuming $H_{dep} \approx 1000\ Oe$ and asking for $L_{\rm opt}, h_{\rm opt} > 1\ \mu m$, we get the condition $H \lesssim 0.4\ Oe$ at room temperature. For such fields, $S_{\rm opt} = h_{\rm opt} \times L_{\rm opt} \lesssim 40\ \mu m \times 1\ \mu m = 40\ \mu m^2$ and the average domain wall velocity drops below $1nm/s$, as is found by extrapolating from the creep law. At such small velocities, which are in principle still measurable (e.g. $v_{min} = 0.01\ nm/s$ in [3]), the "granularity" of creep events should become observable, opening the possibility to test our predictions of spatio-temporal correlations and non-trivial distributions for them.

It is worth mentioning that $L_{\rm opt}$ was also estimated independently in Ta(5.0-nm)/Pt(2.5-nm)/Co90Fe10 (0.3-nm)/Pt(1.0-nm) film wires with perpendicular magnetic anisotropy [33], with a completely different method. Once more, $L_{\rm opt}$ was shown to scale as predicted for the RB $1d$ model with short-range elasticity $L_{\rm opt} \sim H^{-0.75}$. This was achieved by observing the onset of finite effects in the velocity force characteristics at the creep regime, as the wire width w was physically reduced up to $w \sim L_{\rm opt}(H)$ and below. For these samples a field of $H = 16\ Oe$ gives $L_{\rm opt} \approx 0.16\ \mu m$, remarkably in good agreement with the above estimate for the $Pt/Co/Pt$ film. Interestingly enough, our results imply that at low fields, such that $L_{\rm opt} > w$, the velocity is controlled by a power law distribution of thermally activated events with a size cut-off w. This is consistent with the results reported in [33] showing the scaling of the velocity with w in place of $L_{\rm opt}$. Moreover, our findings also predicts that the so-called "zero dimensional" regime in [33] has actually contributions from smaller, power-law distributed, correlated events.

Finally, we note that the characteristic scale $L_{\rm anh}$ may also have a relevance for experiments. As pointed out, we expect a breakdown of the harmonic elasticity of the

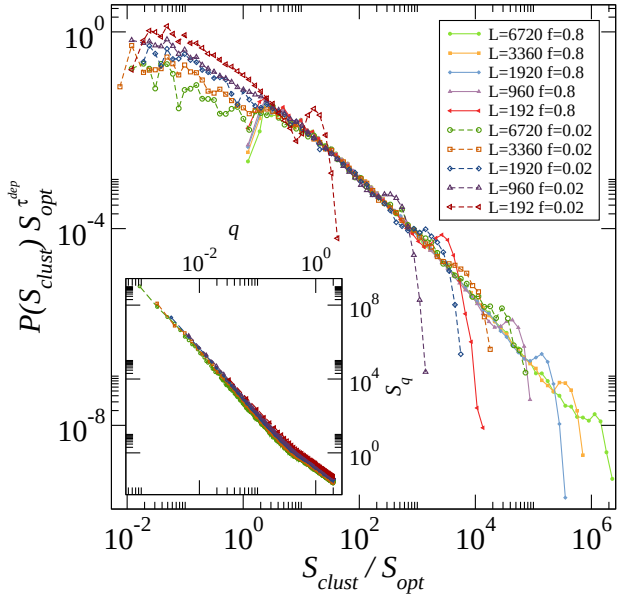

FIG. S8: *Main panel*: Finite size analysis of $P(S_{\rm clust})$ for two different forces, $f = 0.02$ (open symbols) and $f = 0.8$ (filled symbols). System sizes $L \in \{192, 960, 1920, 3360, 6720\}$ are shown. One clearly sees how the growing clusters accumulate at the cutoff "bump" for each force, which also strongly perturbs the sampling of the equilibrium regime, shifting vertically the asymptotic power-law. Nevertheless, this bump is weaker as system size increases, as we expected. *Inset*: Structure factor for $f = 0.02$ and the same several systems sizes as in the main panel, showing consistency.

pure QEW model in one dimension at $L_{\rm anh}$. Although we have considered the effect of a hard-constraint in the elasticity, which drives the system from the $1d$-QEW to the $1d$-QKPZ elastic universality class above $L_{\rm anh}$, the same estimate can be used *a priori* to assess the crossover out of a purely constant elastic behavior, be it to a regime with a softer elasticity or event to one with plastic deformation. Interestingly, in the latter case $L_{\rm anh}$ may represent a typical distance between topological defects on the domain wall. Using Eq.S9 and our estimate for $L_{\rm opt}$ for Pt/Co/Pt thin films of Ref. [34] we get

$$L_{\rm anh} \approx a^{-1} 640\ nm (H_{dep}/H)^{1.75}. \qquad \text{(S14)}$$

where a is approximately the threshold gradient $|dh/dx|$ for harmonic elasticity. Assuming $a \sim 1$ which arises naturally from the harmonic approximation to the line tension energy $\int dx \sqrt{1+|dh/dx|^2} \sim \int dx\ (1+|dh/dx|^2/2)$, we see that deep in the creep regime $L_{\rm anh} \gg L_{\rm opt}$ (e.g. $L_{\rm anh}/L_{\rm opt} \approx 1600$ for $H = 10Oe$ and $H_{dep} \approx 1000\ Oe$ at room temperature [34]). Thus the domain growth rate is still controlled by the ultra-slow elastic creep processes that we describe in this article. This may be the explanation behind the fact that several experiments show consistence with the $1d$-RB-QEW model [33, 34, 41] in spite of the asymptotic "unphysical" properties of the model at large scales. To test this picture it would be important to identify $L_{\rm anh}$ experimentally.

G. MOVIE

Accompanying this supporting information we provide a movie illustrating the spatio-temporal patterns in ultra slow creep dynamics as obtained directly from our simulations for a small $L = 512$ system. The movie displays the sequence of events in space and the activity map, as shown in Fig.1 in the main text.